Magnetic Microtweezers: A Tool for High-Throughput Bioseparation in Sub-Nanoliter Droplets

Simon Dumas, Mathilde Richerd, Marco Serra, Stéphanie Descroix

ADVANCED MATERIALS TECHNOLOGIES
www.advmattechnol.de

Magnetic Microtweezers: A Tool for High-Throughput Bioseparation in Sub-Nanoliter Droplets

*Simon Dumas, Mathilde Richerd, Marco Serra, and Stéphanie Descroix**

Droplet microfluidics has revolutionized the field of single-cell analysis. Production of micro-droplets at high throughput allows for rapid isolation of single cells within micro-compartments, which are then subjected to different analytical processes. However, certain operations, such as physical separation from droplets, remain difficult to implement at high throughput and single-cell level but would be highly valuable to currently expanding multiomics techniques, where several biomolecular modalities are involved. This work presents a method based on microfabricated NiFe structures, the magnetic microtweezers, to trap and extract magnetic particles from a continuous stream of sub-nanoliter droplets, and enable physical separation from single cell-based droplets. Using a physical model, simulations, and experiments, a comprehensive description of the complex particle extraction process is provided. After optimization, the magnetic microtweezers provided unprecedented particle extraction performance, allowing extraction of high loads (10-20 ng) of magnetic particles from 500 pL droplets, with a capture rate close to 100% at 20 Hz. To evaluate the applicability to single-cell analysis, mRNA extraction is performed. It demonstrated around 72% specific recovery of mRNA from droplets containing purified nucleic acids, and 43% from single cells. Overall, this approach enables efficient physical separation that is compatible with existing high-throughput droplet-based single-cell workflows.

1. Introduction

Single-cell sequencing has profoundly modified our vision of life science by offering a comprehensive picture of the molecular landscapes in tissues at the single-cell resolution, which has enhanced our understanding of intracellular heterogeneity, cell lineages, and enabled the discovery of rare cell subpopulations in various contexts such as tumors.[1] In the past decade, single-cell sequencing technologies have undergone remarkable expansion due to advances in next-generation sequencing and microfluidics, and new methods for the study of different cellular modalities, including transcriptomics, genomics, proteomics, and epigenomics, are constantly emerging.[2] Most of these techniques rely on high-throughput cell compartmentalization within micro-droplets, in which the target biomolecule is associated with a unique DNA barcode before being sequenced.[3,4] These technological advances have paved the way toward the development of new methods to address fundamental questions in multiple fields of biology and medicine.[2]

In conjunction with these developments, interest in establishing the links between the various modalities (or omics) present in each cell has dramatically increased in recent years.[5] Such investigations require complex multimodal (or multiomics) methods in which the different modalities are either analyzed in parallel, or sequentially by physical separation of the biomolecules prior to their independent processing. Yet, only the first approach has successfully been adapted to a high-throughput droplet microfluidics format, whereby the various biomolecular processes are performed simultaneously within the droplets, with no additional manipulation required.[6–9] However, these methods remain limited to very few combinations of modalities, including mRNA/surface proteins[6–8] or mRNA/chromatin accessibility,[9] and suffer from a lack of adaptability. In contrast, physical separation-based methods (magnetic particles[10] or cytoplasm/nucleus isolation[11]) can enable very versatile workflows that can be easily extended to multiple modalities, but remain labor intensive and are generally limited to analyses of only a few cells. Thus, in this context, implementing a physical separation step at the single-cell level in droplet format would provide the advantages of versatility and scalability, and offer new perspectives for single-cell multimodal analysis.

Many research groups in the field of microfluidics have been working on the implementation of magnetic particle separation in droplets.[12] Examples include methods based on attracting magnetic particles to one side of the droplet prior asymmetric splitting at a junction.[13–15] While this strategy is compatible with high-throughput approaches, the purification rates are sub-optimal due to a significant loss of droplet volume after purification. Other technologies based on electrowetting[16,17] or

S. Dumas, M. Richerd, M. Serra, S. Descroix
Institut Curie
Laboratoire PhysicoChimie (CNRS UMR 168)
Institut Pierre-Gilles de Gennes
Sorbonne Université
PSL Research University
6 rue Jean Calvin, Paris 75005, France
E-mail: stephanie.descroix@curie.fr

The ORCID identification number(s) for the author(s) of this article can be found under https://doi.org/10.1002/admt.202200747.

DOI: 10.1002/admt.202200747

droplet arrays[18] offer good performance and control, but are not suitable for high-throughput assays. Our group previously proposed an original approach in which external[19,20] or integrated[21,22] magnetic tweezers are used to extract and redisperse magnetic particles from droplet to droplet with a high purification rate. Although powerful, these technologies could only operate at low throughput (≈1 Hz) and with large droplet volumes (≈10^2 nL); thus, are not compatible with single-cell analysis where a high throughput (10–100 Hz) and small droplets (<1 nL) are generally required. Therefore, with the goal of opening new avenues of single-cell analysis, the purpose of the current work was to develop a new approach based on magnetic microtweezers to enable high-throughput physical separation at the sub-nanoliter range.

Development of the proposed single-cell technology requires us to downscale the current magnetic tweezer approaches by at least two orders of magnitude. However, miniaturization leads to dramatic changes in the balance between the involved forces. At small scales, capillary forces predominate over magnetic forces, which compromise droplet breakup and thus the extraction of particles from the droplets. Here, we develop a new generation of magnetic microtweezers consisting of microfabricated NiFe soft magnets integrated in a microfluidic chip. These structures, referred to as magnetic microtweezers, are precisely positioned on each side of a microfluidic channel to focus the magnetic field of an external permanent magnet. This produces a strong magnetic force that can trap and extract magnetic particles from sub-nanoliter droplets. Based on theoretical, numerical, and experimental analyses, we show that these new magnetic microtweezers can extract high loads of magnetic particles from droplets of only 500 pL. We then demonstrate the potential of the magnetic microtweezers for high-throughput physical separation of biomolecules from biological samples, in particular, from single cells.

2. Results and Discussion

2.1. Design of the Magnetic Microtweezers

To ensure that the magnetic tweezers approach is compatible with sub-nanoliter droplets, the dimensions of the system must be two orders of magnitude smaller than existing magnetic tweezer-based devices. However, at this scale, the predominance of capillary forces over magnetic forces could compromise particle extraction. We can easily demonstrate that the force ratio scales with $F_{\text{magnetic}}/F_{\text{capillary}} \propto \text{Volume}^{2/3}$ (Equation (SA.1), Supporting Information), meaning that reducing the droplet volume by two orders of magnitude would be practically equivalent to a ≈20-fold decrease in magnetic force. To overcome this limitation, we designed new magnetic microtweezers to maximize the magnetic force. These microtweezers consist of two magnetic tips facing each other across a microfluidic channel that transports the droplets. This geometry focuses the magnetic field lines in a given channel region, which generates a high local magnetic field gradient, thus guaranteeing effective trapping of magnetic objects (**Figure 1**a–c).[19,21,23] Previous microfluidic devices based on magnetic tweezers were limited to magnetic field gradients as low as 430–500 T m^{-1},[19,21] which is incompatible with sub-nanoliter droplets—where interfacial forces predominate (Equation (SA.2), Supporting Information). Such low gradients were either due to an excessive distance (>100 µm) between the tweezers and the microfluidic channel,[19] or the choice of a poorly magnetizable (Bsat = 0.3 T) material for the tweezers.[21]

To develop the next generation of magnetic tweezers, we opted for a microfabrication method based on NiFe (permalloy) electroplating[24,25] and soft lithography. This method allows the production of highly magnetizable structures in combination with fine control of their positioning[26] in very close proximity (from 8 to 15 µm) to the microfluidic channel (Figure 1d). Using this method, we achieved the fabrication of 35 µm-thick metal structures on glass slides. These structures had a Ni:Fe ratio of 80:20, as determined by energy-dispersive X-Ray spectroscopy (Figure S1, Supporting Information). We extracted the magnetization curve of the structures (Figure S2, Supporting Information) through vibrating sample magnetometry, and obtained a magnetization at saturation value (Bsat) of 0.93 T, which is comparable with the values reported in previous studies using a similar electrodeposition method.[24,25]

Conception of this device was assisted by finite-element simulations of the magnetic field, with the aim to maximize the intensity, gradient, and spatial distribution of the magnetic field between the tips. An example of the magnetic profile generated by the proposed method is shown in **Figure 2**. Here, an external cubic neodymium magnet (remanence Br = 1.43 T) with sides of 5 mm was placed 3 mm away from the tweezers. The electroplated tweezers consist of two 35 µm-thick triangles with a base and height of 400 µm, spaced 60 µm apart from each other (Figure 2a). The microfluidic channel section is 35 × 30 µm, which confines the droplets as they pass through the tweezers (e.g., an aspect ratio of 15:1 for a 500 pL droplet).

The simulations clearly suggested that the magnetic microtweezers focused the magnetic field lines (Figure 2a), yielding a maximum field intensity of around 0.5 T in the microfluidic channel between the tips (Figure 2b). With the force being oriented in the direction of increasing field intensity, these simulations confirmed attraction of the particles toward the tips. Next, we computed the magnetic field gradients (Figure 2b) to determine the intensity of the magnetic force. Strikingly, the maximum gradient value in the channel is around 11 000 T m^{-1}, which is ≈22 times higher than in previous devices.[19,21] This gradient would generate a magnetic force of ≈2 µN on the aggregate of magnetic particles, which would overcome the interfacial force of ≈0.4 µN and thus enable extraction of the aggregate of magnetic particles (Equation (SA.3), Supporting Information). Additional simulations showing the process of geometry optimization are provided in Figure S3a–c (Supporting Information).

2.2. Physics of the Capture of Magnetic Particles

The process of magnetic particle extraction is characterized by three distinct stages. First, in the cluster formation stage, the particles present in the droplet migrate and are trapped between the tweezers to form a compact cluster (**Figure 3**a). Then, the cluster is extracted out of the droplet and remains trapped between the tweezers (Figure 3b). Finally, the cluster is released and pushed away by the following droplet, and the next

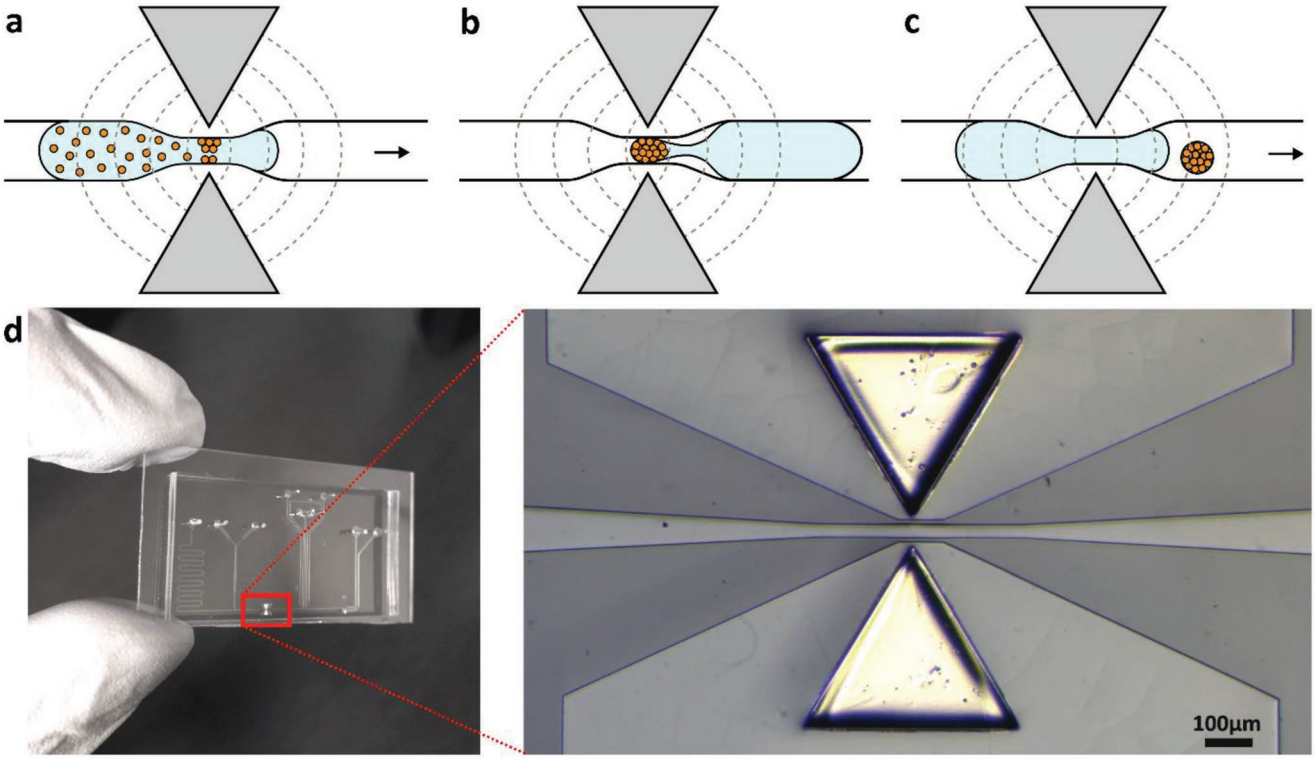

Figure 1. Integrated magnetic microtweezers. Principle of magnetic particle extraction. a) The tweezers collect the particles present in a droplet, and the collected particles form an aggregate. b) The aggregate remains trapped between the tweezers and is extracted from the droplet. c) The following droplet pushes the aggregate out of the tweezers, to allow the particles in the next droplet to be extracted. d) Left: Device overview. The tweezers are encompassed in the red box. Right: Micrograph of the magnetic microtweezers in the chip. The microfluidic channel (cross section, 30 × 35 µm) is separated from the magnetic tips by a thin PDMS membrane of ≈8 µm.

extraction can proceed (Figure 3c). In order to both determine the critical parameters of the extraction process and to predict the working range of the device, we derived three simple theoretical criteria, each describing the balance of forces at each specific stage.

2.2.1. Cluster Formation Criterion

The magnetic force acting on a single magnetic particle (≈pN)[27] is several orders of magnitude smaller than the interfacial forces within the droplet in which the particle is dispersed (≈µN). Therefore, in order to extract the particles, a compact aggregate of the particles, named here "cluster," must be generated to increase the effective magnetic force. Under the magnetic field generated by the tweezers, a magnetic particle in a droplet is subjected to two opposing forces: the magnetic force holding the particle between the tweezers, and a viscous drag force (Stokes force) pushing the particle in the direction of droplet displacement (Figure 3a). The ratio of these two forces provides a criterion to characterize cluster formation ($F_{mag}/F_{drag} > 1$).

However, this initial criterion does not take into account magnetic interactions between the particles.[28] Under a magnetic field, the magnetic particles arrange into columns aligned with the field due to dipole–dipole interactions, and these arrangements are transported as a whole and act as larger, non-spherical objects. This phenomenon, referred to as "cooperative magnetophoresis,"[29–31] leads to increased magnetophoretic velocity and facilitates further aggregation of magnetic particles. The magnetic force acting on a column of beads is assumed to be equal to the sum of the force applied to each individual particle, as this body force acts in the bulk of the material, and can be expressed as:

$$F_{mag,column} = N\rho_p V_p M_p \nabla B \quad (1)$$

where N is the number of particles in the column that can be estimated experimentally, ρ_p (kg m^{-3}) and V_p (m^3) are the particle density and volume, respectively, M_p (emu g^{-1} or A m^2 kg^{-1}) is the particle magnetization per mass unit, and ∇B (T m^{-1}) is the magnetic field gradient. The Stokes drag force also needs to be modified to consider the shape and orientation of the bead columns. For a column of N beads oriented perpendicular to the flow, the Stokes drag force can be expressed as[32]:

$$F^{\perp}_{drag,column} = -\xi_{\perp} 6\pi\eta r_p u_{\perp} \quad \text{with} \quad \xi_{\perp} = \frac{4}{3}\frac{N}{\log N + \gamma_{\perp}} \quad (2)$$

where η (Pa s) is the droplet viscosity, r_p (m) is the particle radius, $u_{\perp}$ (m s^{-1}) is the relative velocity between the particle column and the droplet, and $\gamma_{\perp}$ is a correction factor estimated to be around 1.111.[32] Hence, we can provide a more realistic

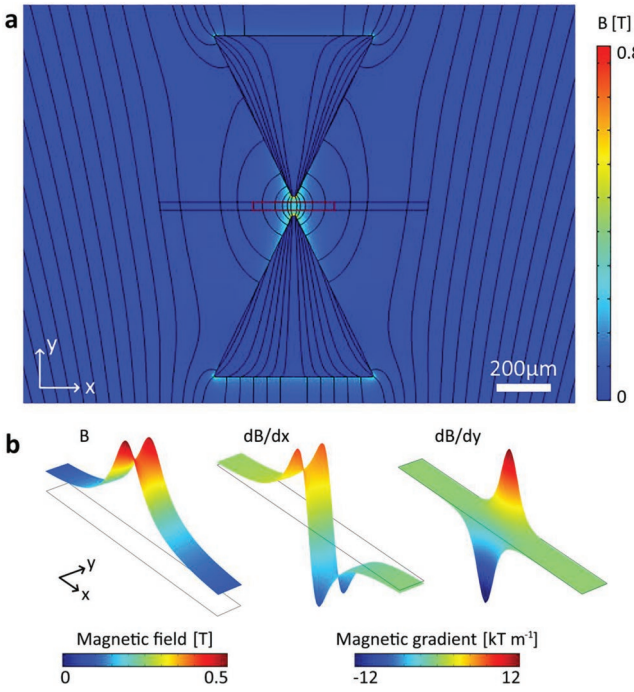

Figure 2. Results of the magnetic field simulation. a) Magnetic field lines and intensity around the magnetic microtweezers. The external field is generated by an external permanent magnet (5 mm cube, Br = 1.43 T) placed 3 mm away from the tweezers. b) Magnetic field and gradients in the channel. The values were extracted for a small section of the channel, represented by the red rectangle in (a). Additional simulation results showing the geometry optimization are provided in Figure S3 (Supporting Information).

criterion for cluster formation by calculating the ratio between Equations (1) and (2):

$$\frac{F_{\text{mag,column}}}{F^{\perp}_{\text{drag,column}}} = \frac{\rho_p r_p^2 \left(\log N + \gamma_{\perp}\right) M_p \nabla B}{6\eta u_{\perp}} \tag{3}$$

2.2.2. Droplet Breakup Criterion

Once formed, the next step is to extract the aggregated particles from the droplet. This operation is governed by the balance between magnetic and interfacial forces (Figure 3b). Capillary force, which opposes droplet breakup, can be estimated by the Laplace law.[19] For a cluster occupying the whole channel cross-section L^2, capillary force is equal to:

$$F_{\text{cap}} = 4\gamma L \tag{4}$$

where γ (N m^{-1}) is the interfacial tension. The magnetic force applied on the cluster can be expressed as a function of the cluster volume, using:

$$F_{\text{mag,cluster}} = \rho_p \phi V_c M_p \nabla B \tag{5}$$

where V_c (m^3) is the cluster volume and ϕ is the volume fraction of particles within the cluster, also referred to as compacity, which is around 0.5–0.6 for randomly close-packed spherical particles.[33] Therefore, a second criterion can be defined as the ratio between magnetic (Equation (4)) and capillary (Equation (5)) forces for a spherical cluster occupying the whole channel cross-section, as follows:

$$\frac{F_{\text{mag,cluster}}}{F_{\text{cap}}} = \frac{\rho_p \phi L^2 M_p \nabla B}{24\gamma} \tag{6}$$

As for cluster formation, this ratio must remain over 1 to ensure droplet breakup.

2.2.3. Cluster Release Criterion

The cluster capture and release operations of previously reported technologies[19,21] require active control over the magnetic field, and rely on synchronization of the displacement of the permanent magnet and the droplet flow. This strategy is unpractical at high throughput.[21] To avoid such synchronization, we propose a passive method in which the cluster is pushed out of the tweezers region by the following droplet (Figure 3c). This is made possible by the presence of fluorosurfactants in the carrier oil, which prevents the droplets from coalescing via steric repulsion. However, this "pushing" force must overcome the magnetic force that holds the cluster in place. When the next droplet makes contact with the cluster, the interfaces of both droplets will be compressed, which reduces the gap left for oil to flow around the droplets, resulting in a downstream increase in pressure. In the worst-case scenario where the entire circulation is blocked, the downstream pressure will equal the inlet pressure, and a force can be derived from the pressure difference across the packed droplet-cluster plug, as follows:

$$F_{\text{pressure}} = L^2 \left(P_{\text{in}} - P_{\text{out}}\right) \tag{7}$$

By determining the ratio between this pressure force (Equation (7)) and the magnetic force on the cluster (Equation (5)), we can provide our last criterion, which allows us to determine the minimum required inlet pressure to ensure passive, effective release of the cluster.

$$\frac{F_{\text{pressure}}}{F_{\text{mag,cluster}}} = \frac{6\left(P_{\text{in}} - P_{\text{out}}\right)}{\rho_p \phi \pi L M_p \nabla B} \tag{8}$$

2.2.4. Evaluation of the Working Range of the Device Using Theoretical Criteria

We next used the three theoretical criteria established above (Equations (3), (6), (8)) to determine the critical parameters that are pivotal to ensure good operation of this device. In particular, we calculated these three criteria to estimate the theoretical device operating conditions in terms of velocity, channel dimension, and pressure, respectively (Table S1, Supporting Information, Figure 3d–f). All other quantities present in the equations were taken from either the literature, simulations, measurements, or from our specifications (numerical values available in

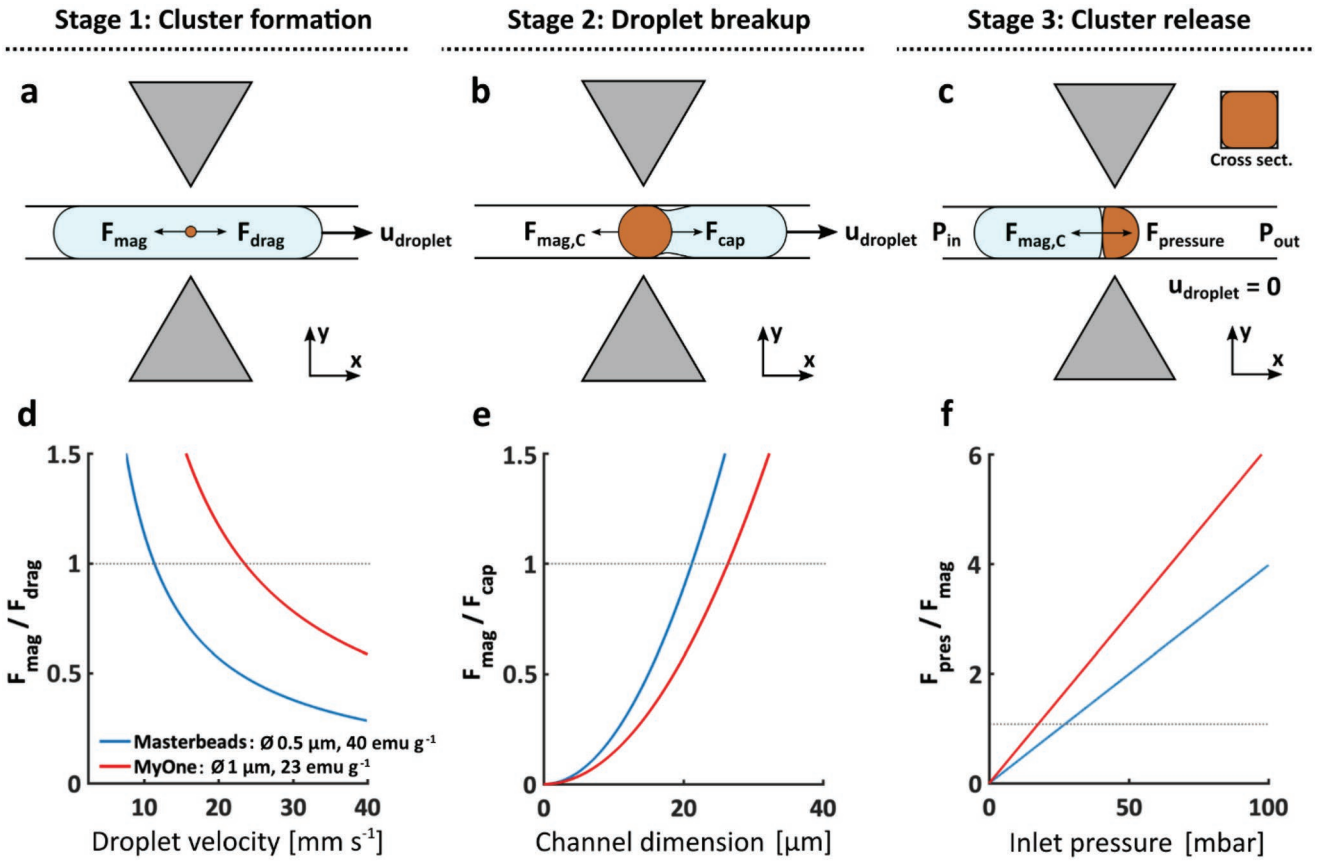

Figure 3. The three stages of extraction of magnetic particles from droplets by the magnetic microtweezers. a) Cluster formation. b) Droplet breakup. c) Cluster release. F_{mag} and $F_{mag,C}$ correspond to the magnetic force applied on a single particle, and on the cluster of particles, respectively. F_{cap} is the capillary force, $F_{pressure}$ is the force applied by a following droplet on the cluster of particles. These forces are detailed in Section 2.2, and Equations (1)–(8). d–f) Estimation of the force ratio at each stage; these force ratios were used as a criteria to estimate the working range (velocity, dimensions, inlet pressure) of the device. The force ratio at each stage must be over 1 (gray line) to ensure proper operation of the device. The force ratios were calculated for two types of magnetic particles: Masterbeads (Ademtech, size 0.5 µm, Ms = 40 emu g^{-1}; blue lines) and MyOne (Invitrogen, size 1 µm, Ms = 23 emu g^{-1}; red lines).

Table S1, Supporting Information). We investigated two types of magnetic particles that are commonly used in bioassays: Masterbeads (Ademtech, size 0.5 µm, Ms = 40 emu g^{-1}) and MyOne (Invitrogen, size 1 µm, Ms = 23 emu g^{-1}). Based on the first criterion (Figure 3d), MyOne would allow good cluster formation at a droplet velocity of up to ≈25 mm s^{-1} whereas Masterbeads would work at only ≈12 mm s^{-1}, indicating that the particle size has greater influence on magnetophoresis than magnetization. The second criterion (Figure 3e) suggested that channel dimensions below ≈20 µm would compromise droplet breakup and thus lead to improper cluster extraction. Therefore, we decided to set the dimension of the channel to ≈30–35 µm to ensure droplet breakup. Finally, the last criterion (Figure 3f) suggested that the magnetic cluster could be effectively pushed by the next droplet at an inlet pressure higher than ≈25 mbar, which is within the operating range of our device (typically 30–200 mbar).

2.3. Experimental Characterization of Magnetic Particle Capture

We next experimentally demonstrated the validity of our approach by injecting 450 pL aqueous droplets into the chip, with each droplet containing 18 ng of Masterbeads. **Figure 4** and Video S1 (Supporting Information) show the complete extraction process, demonstrating the ability of our approach to efficiently extract particles from sub-nanoliter droplets. This also confirms the proper operation of the three previously described stages, namely cluster formation (Figure 4a,b), droplet breakup (Figure 4c,d), and cluster release (Figure 4e,f). The device operated in good agreement with the theoretical predictions, as we observed that: (i) capture efficiency decreased as speed increased; (ii) droplet breakup always occurred properly in a channel with a cross section of 30 × 35 µm; and (iii) a minimal pressure of ≈30 mbar was required to achieve cluster release. In these experiments, this minimal pressure corresponded to a typical droplet velocity of below 3 mm s^{-1}.

Under these conditions, the main limiting factor is the droplet velocity, which can only be increased at the expense of capture efficiency, and in turn compromises the high-throughput property of the device. First, we used an automated image acquisition and analysis workflow to quantify the bead capture efficiency (see Experimental Section and Figure S4, Supporting Information). Using the experimental conditions described above (Figure 4), reducing the droplet velocity from

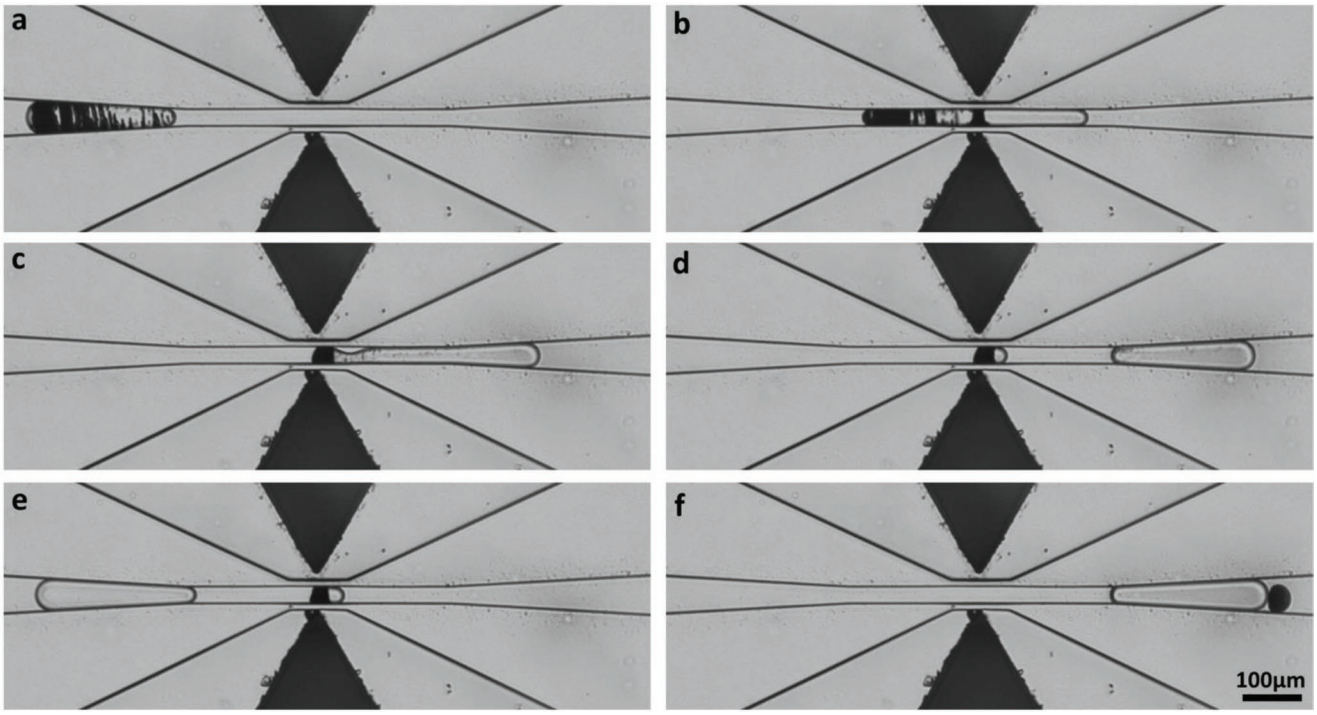

Figure 4. Extraction of 18 ng of Masterbeads from a 450 pL droplet (flow ≈4 mm s^{-1}). We can recognize the three previously described stages: a,b) cluster formation, c,d) droplet breakup, and e,f) cluster release. In this experiment, clusters are pushed by empty PBS droplets, which will be useful for subsequent image analysis (see Experimental Section). The tweezer dimensions are a base and height of 300 µm and thickness of 35 µm (see Video S1, Supporting Information).

4 to 24 mm s^{-1} decreased the bead capture efficiency from 90% to 50% (**Figure 5**). To overcome this limitation, we further optimized the size and shape of the tweezers. We investigated

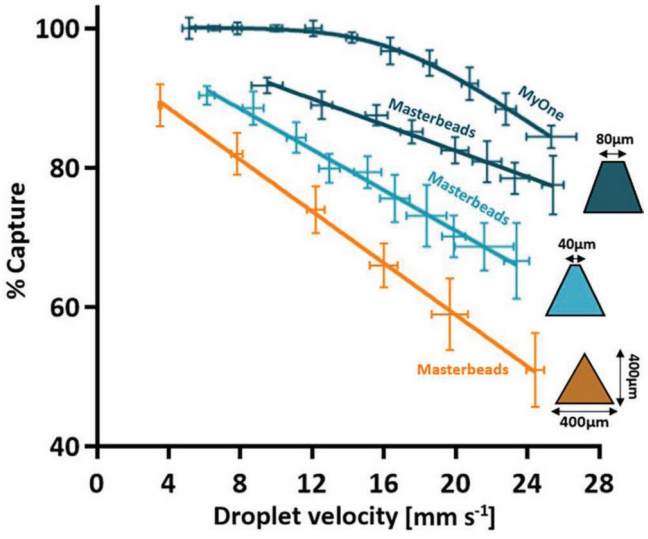

Figure 5. Characterization of the efficiency for different shapes of magnetic microtweezers. The percentage of capture is plotted against droplet velocity. Efficiency decreases with velocity for all conditions. However, trapezoidal tweezers (light and dark blue lines) significantly improve the efficiency compared with triangular tweezers (orange line). Higher efficiencies were observed using MyOne beads compared to Masterbeads, with MyOne beads yielding an efficiency close to 100% for droplets flowing below 12 mm s^{-1} (top dark blue line).

the influence of the size of the tweezers on capture efficiency. Reducing the dimensions (base and height) of the triangular tweezers down to 100 µm lead to a dramatic loss of efficiency, whereas increasing the dimensions from 300 to 400 µm did not bring any significant improvement (Figure S5a, Supporting Information). In contrast, we found that the distance to the permanent magnet had a much more significant influence on capture efficiency, with a ≈50% improvement observed when the distance between the tweezers and the permanent magnet was reduced from 5 to 3 mm (Figure S5b, Supporting Information).

In parallel, we observed that the main cause of particle loss during the extraction process originated from detachment of particles from the magnetic cluster (Figure S5c, Supporting Information). As magnetic attraction is strongest in the immediate vicinity of the tweezers, the particles at the edge of the cluster are subject to weaker magnetic forces, which eventually become insufficient to keep the particles in the cluster when the aggregate reaches a certain size. To avoid such particle loss, we designed trapezoidal tweezers to widen the region of the strong magnetic field to be comparable or wider than the size of the clusters (Figure S5d, Supporting Information). This trapezoid-widening strategy significantly improved the capture efficiency compared to triangular tweezers, from around 50% up to 80% with the droplets flowing at 24 mm s^{-1} (Figure 5a). The simulations were in good agreement, and confirmed that using such trapezoids does not decrease the strength of the magnetic field gradient compared to triangular tweezers, but effectively widens the range of action of the tweezers (Figure S3d, Supporting Information).

We also compared the device performance for two types of beads and found that the use of MyOne (size 1 µm,

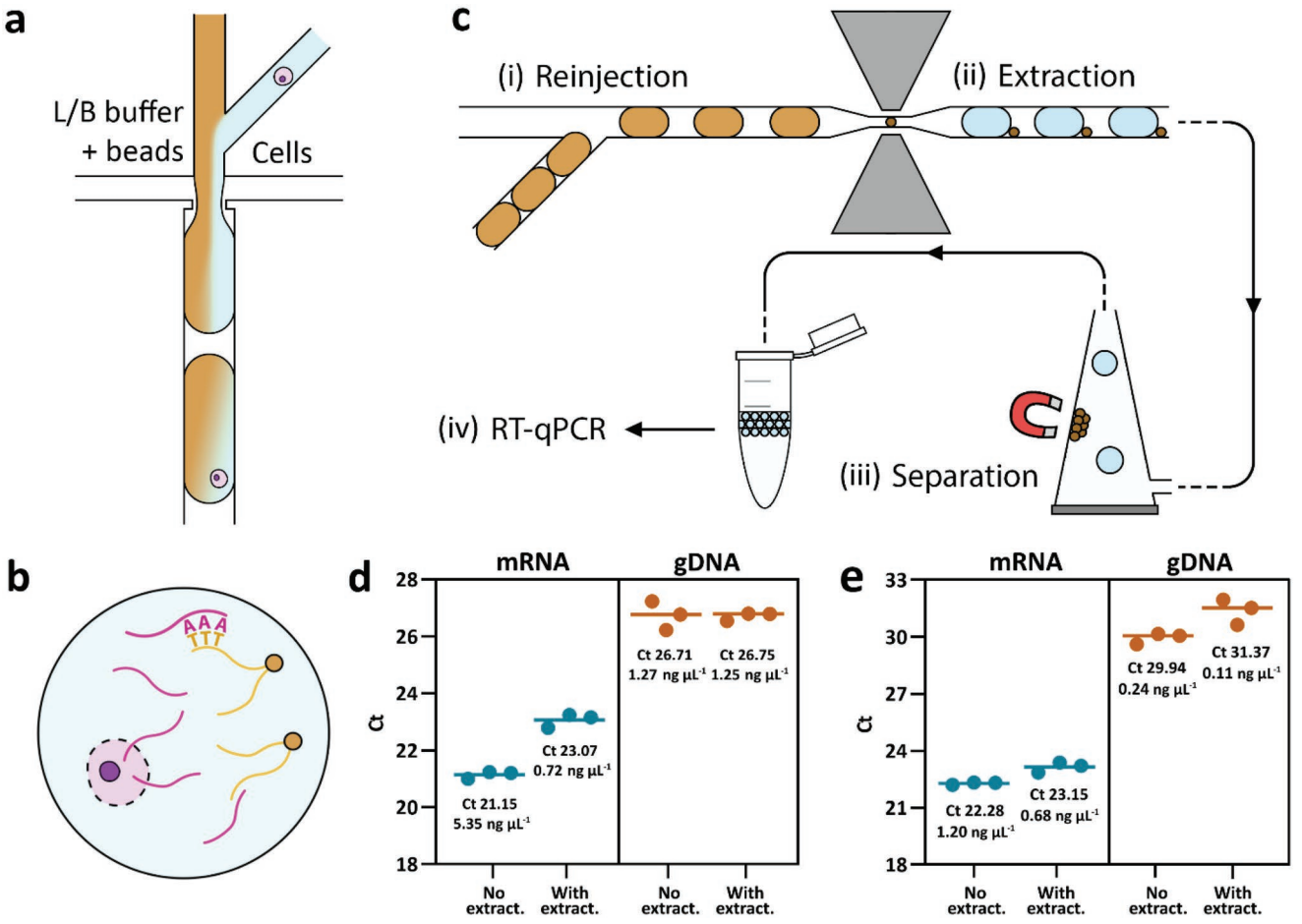

Figure 6. Flowchart of single-cell mRNA extraction using the magnetic microtweezers. a) Cells and Oligo-dT beads were co-encapsulated in droplets of lysis/binding buffer. b) Cell lysis and binding of mRNA to the beads. c) Progression of droplets in the magnetic microtweezer chip: i) the droplets are reinjected and spaced in a stream of oil, ii) the beads are extracted using the tweezers, iii) the bead clusters are separated from the remaining droplets in an intermediary reservoir, and iv) the droplets are collected in a tube before being analyzed via (RT)-qPCR. Results of (RT)-qPCR analysis of the emulsion collected after extraction, compared to an identical emulsion that was not subjected to extraction through the chip. d) (RT)-qPCR results for a sample of purified oligonucleotides. The extraction rates of 72% for mRNA and only 1.7% for gDNA indicate a good purification rate and high specificity. e) (RT)-qPCR results for encapsulated single cells that were not subjected to extraction. The mRNA extraction rate was 43% and 52% of gDNA was non-specifically extracted.

Ms = 23 emu g^{-1}) instead of Masterbeads (size 0.5 µm, Ms = 40 emu g^{-1}) increased the bead capture efficiency even more, with the MyOne beads giving capture percentage close to 100% at velocities between 4 and 12 mm s^{-1} (Figure 5a). This is in good agreement with our theoretical predictions, which showed that the size of the particles has a more significant impact on capture than their magnetization. Ultimately, these new trapezoid-shaped magnetic tweezers combined with MyOne beads resulted in a significant improvement in terms of throughput, with no loss of capture efficiency. Thus, due to these good performance parameters, these magnetic microtweezers may represent a relevant separation technique for low-volume and high-throughput applications such as droplet-based single-cell analysis.

2.4. Purification of mRNA from Biological Samples

To demonstrate the potential of the magnetic microtweezers to perform physical separation of biomolecules, we first extracted mRNA from purified nucleic acids using oligo-dT beads (MyOne Beads conjugated with oligo-dT) in 500 pL droplets. Using a buffer adapted for this bioassay, we achieved efficient bead extraction at a throughput of 20 droplets per second (Video S2, Supporting Information), which represents a significant improvement compared to previous technologies, which were limited to ≈1 Hz. Once the bead extraction was completed, we obtained two distinct droplet families: one containing the beads and potentially the extracted mRNA, and larger non-magnetic droplets containing the remaining solution. The volume of the magnetic droplets was around 13 pL, indicating that supernatant retention was as low as 2.5% of the total droplet volume. As shown in **Figure 6**c, we used a home-made intermediary reservoir equipped with a magnet to specifically sort the magnetic bead-containing droplets from the non-magnetic droplets. To evaluate the performance in terms of physical separation of biomolecules, we pooled the collected emulsion of non-magnetic droplets and quantified mRNA through RT-qPCR. The percentage of mRNA extraction was evaluated by

comparing the results of RT-qPCR on the emulsions before and after separation of the magnetic particles.

Under these conditions, our device showed a high extraction efficiency of around 72% for mRNA, corresponding to a decrease in the total mRNA concentration in non-magnetic droplets from 5.53 to 0.72 ng μL^{-1} (Figure 6d). To further assess the multimodal (or multiomic) potential of our method, we evaluated the specificity of the purification by measuring, in parallel, the quantity of gDNA in the emulsions. The gDNA was only depleted from 1.27 to 1.25 ng μL^{-1} for the purified nucleic acid sample, corresponding to a non-specific gDNA extraction rate as low as 1.7%. These results indicate the magnetic microtweezers offer very good mRNA separation efficiency and specificity for purified nucleic acid samples (Figure 6d).

We next applied the magnetic microtweezer approach to single-cell analysis by encapsulating single cells (MDA-MB-231 breast cancer cells) in droplets. Using a conventional flow-focusing microfluidic device, we co-encapsulated a cell suspension (200 cell μL^{-1}) in 500 pL droplets using a lysis/binding buffer containing MyOne beads conjugated with oligo-dT (Figure 6a). Under these conditions, around 10% of the droplets contained a cell. The single cells were lysed within the droplets, and the released mRNA specifically binds to the beads (Figure 6b). To properly lyse the cells while maintaining droplet stability, the droplets contained Triton X-100 at 0.05% *v/v*. This detergent concentration is rather low compared to conventional lysis buffers; therefore, we validated that such a low detergent concentration promoted efficient release of mRNA from the cells (Equation (SB.1), Supporting Information).

We then reinjected the collected emulsion onto the magnetic microtweezer chip to extract the particles from the droplets and physically separate the mRNA from the other cellular components present in the cell lysate (Figure 6c,i–ii). As before, the magnetic and non-magnetic droplets were sorted, and the mRNA and gDNA contents of the non-magnetic droplets were evaluated by (RT)-qPCR.

Efficient physical separation of biomolecules from single cells was accomplished, as we achieved a capture efficiency of 43%, with the total mRNA concentration decreasing from 1.20 to 0.68 ng μL^{-1} (Figure 6e). The lower efficiency compared to the experiments performed on purified nucleic acid samples was expected, as non-specific binding or RNA degradation are more likely to occur with complex samples, such as cell lysates. Furthermore, around 52% of gDNA was non-specifically extracted on the beads (Figure 6e), which suggests a lower specificity of mRNA extraction from single cells than from the purified nucleic acids. These important differences in the purification rate and specificity between these two samples may arise for a variety of diverse reasons, including the very low quantities of material in single-cell lysates, non-specific interactions with various released cellular components, or possibly incomplete cell lysis or DNA unfolding during cell encapsulation and lysis. These issues represent targets for future optimization (e.g., buffer composition, lysis conditions, proteinase digestion, type of beads) to improve the extraction yield and specificity. However, despite the lower efficiency of biomolecule capture when using single cells, the quantity of mRNA recovered using the magnetic microtweezers is still sufficient for downstream sequencing, as current commercial droplet-based single-cell sequencing platforms only capture 6.7–32% of the transcripts present in each cell.[34]

3. Conclusion

We developed a new method that enables the extraction of magnetic microparticles from a continuous flow of sub-nanoliter droplets at high throughput that is compatible with single-cell applications. This approach is based on microfabricated NiFe structures, namely the magnetic microtweezers, which focus an external magnetic field in a narrow region of the channel. This leads to high magnetic gradients in the channel, up to 11 000 T m^{-1}, which are more than 20 times higher than previous technologies.[19,21] The resulting strong magnetic force attracts and traps the magnetic particles present in sub-nanoliter droplets flowing through the channel, and ultimately leads to droplet breakup, isolating the aggregated particles from the rest of the droplet.

These magnetic microtweezers demonstrated unprecedented magnetic particle extraction performance in terms of throughput, extraction percentage, and particle loading. A bead extraction efficiency close to 100% was achieved on 450 pL droplets containing 18 ng of MyOne particles (12 000–18 000 beads) at a throughput of 20 droplets per second. In comparison, other extraction technologies are limited to either a low throughput (≈1 Hz) and large droplets (>100 nL),[19,21] or have a high throughput but low particle loading and high sample loss.[13–15]

Due to these unique functionalities, the magnetic microtweezers could be adapted to high-throughput droplet-based single-cell analysis, particularly in the context of multiomics studies where physical separation of different biomolecular modalities would greatly facilitate subsequent biomolecular processing. Therefore, we employed the magnetic microtweezers to extract mRNA using oligo-dT magnetic particles. When using a purified nucleic acid solution as the sample, the device demonstrated an efficient mRNA extraction rate of 72%, and excellent specificity as only 1.7% of the gDNA was extracted. When using single cells as the sample, the mRNA extraction rate decreased to 43% and 52% of gDNA was non-specifically extracted. Although these performances could certainly be improved in the future by optimizing the lysis buffer and RNA binding conditions, the quantities of material recovered are sufficient for downstream sequencing.

Overall, these very promising results demonstrate for the first time that physical separation is possible at the single-cell level in droplets at high-throughput. We envision the magnetic microtweezers could confer this functionality to multistep droplet microfluidic workflows (e.g., by including a washing step, barcoding strategy, or reagent addition step), and would ultimately enable new multimodal single-cell protocols to be performed in the droplet format for applications where maximizing recovery of the biomolecules is crucial.

4. Experimental Section

Preparation of Micro-Magnetic Substrates: Micro-magnets were fabricated by NiFe (permalloy) electroplating using photoresist

molds. First, a Ti–Cu seed layer was evaporated by sputtering (Plasmionique) on glass slides (75 × 50 mm, Corning) to render the slides conductive. TI-Prime (Microchemicals) was then applied to promote photoresist adhesion, after which the negative-tone photoresist AZ-125nXT (Microchemicals) was spun and processed via standard photolithography (MJB4 Mask Aligner, Süss MicroTec) to leave bare copper where the soft magnets were to be grown. Permalloy plating was performed as previously described[25,35] in a bath containing $NiSO_4{\cdot}7H_2O$ (250 g L^{-1}), $FeSO_4{\cdot}7H_2O$ (5 g L^{-1}), boric acid (25 g L^{-1}), saccharin (1 g L^{-1}), and sodium dodecyl sulfate (0.1 g L^{-1}). Electrodeposition was carried out at 30 °C with magnetic stirring over ≈12 h with a current density of 7 mA cm^{-2} to reach an average thickness of 35 µm. After deposition, the substrates were immersed in heated TechniStrip P1316 (Technic) until the photoresist and copper completely dissolved. However, the titanium seed layer could not be removed without the use of dangerous solvents such as HF. Thus, an additional surface treatment was performed as an alternative to titanium etching, and enabled subsequent PDMS bonding and silanization. After oxygen plasma activation, the substrates were exposed to tetraethyl orthosilicate (TEOS) through vapor deposition under vacuum for 20 min to supplement the oxidized titanium layer with silanol groups, which noticeably improved further PDMS plasma bonding.

Micro-Magnet Characterization: The chemical composition of the micro-magnet structures was determined (Figure S1, Supporting Information) through energy-dispersive X-ray spectrometry. The magnetization curve (Figure S2, Supporting Information) was extracted using a vibrating sample magnetometer on permalloy disks (diameter, 800 µm; thickness, 35 µm) and corrected for demagnetizing fields using an analytical correction factor for disks.[35]

PDMS Chip Fabrication, Alignment, and Bonding: PDMS chips were fabricated through standard soft lithography on photoresist molds, using SU-8 2035 (Microchem) on 4″ silicon wafers to obtain 35-µm-thick patterns and PDMS (polydimethylsiloxane, Sylgard 168) at a curing agent ratio of 1:10. To ensure the flatness of the chips, the molds were placed in a home-made sarcophagus before pouring and cross-linking PDMS, as described previously.[26] The PDMS slabs and micro-magnet substrates were O_2 plasma-activated, then precisely aligned and bonded together using a mask aligner (MJB4, Süss MicroTec), as described previously.[26,36]

Magnetic Field Simulations: The Magnetic Field No Currents module of COMSOL Multiphysics 5.5 was used for the magnetic field simulations. The magnetic tweezers and the cubic external magnet with sides of 5 mm (placed at a distance of 3–7 mm from the tweezers) were drawn in 3D. The measured magnetization curve (Figure S1, Supporting Information) was set as a material property for the tweezers and a remanence flux density of 1.43 T was set for the permanent magnet, as specified by the magnet supplier (Supermagnete). The surrounding volume (PDMS, channel, and air) was set as a non-interacting medium (μ_r = 1). A mesh refinement study was performed to ensure that the results were not mesh-dependent (data not shown).

Microfluidic Device Operation: Magnetic beads (MyOne, Invitrogen or Masterbeads, Ademtech) were washed four times in PBS, resuspended at 40 µg $µL^{-1}$ in PBS, and emulsified in a flow-focusing microfluidic chip using a syringe pump (Nemesys, Cetoni) or a pressure controller (MFCS, Fluigent) and Novec-7500 (3 M) containing 2% *w/w* Fluosurf surfactant (Emulseo) as a carrier oil. Fine droplet size monitoring was achieved by real-time measurement through image analysis with a custom LabView program. A droplet volume of 450 pL led to a loading of 18 ng of beads in each droplet. The emulsions were kept in home-made reservoirs, then reinjected to the magnetic microtweezer chip. For the capture efficiency characterization experiments, droplets containing particles and pure PBS droplets were reinjected alternatively using a previously described droplet pairing strategy.[37] A neodymium cubic permanent magnet (Supermagnete) with sides of 5 mm and remanence of 1.43 T was placed using a 3D-printed holder at a distance from 3 to 5 mm from the tweezers, vertically centered with the channel plane.

Image Acquisition: Droplet images were captured using a digital camera (Basler Ace USB 3.0) mounted on an inverted microscope (Zeiss Axiovert 200). A home-made LabView program was used to automatically take pictures whenever a droplet crosses the field of view. For each flow rate condition, images of droplets were acquired from the regions both before and after the extraction area to be compared in a further image analysis procedure. Videos of moving droplets (frame rate 50 fps) were also taken for each flow rate condition to evaluate the velocity of the droplets via image analysis. High-speed videos (Video S2, Supporting Information) were taken using a Phantom v4.2 camera.

Image Analysis: After automatized background removal and trimming through a MATLAB program, the pixel intensity was quantified for each droplet (Figure S4, Supporting Information). To evaluate capture efficiency, a linear relationship between the pixel intensity and droplet particle loading was assumed; however, this assumption is imperfect at high loadings where many particles are stacked in the *z*-axis, and must provide more accurate results at low particle concentrations. Although not ideal, it seemed reasonable to consider that the droplets are largely flattened in the visualization area (35-µm-thick, 120-µm-wide), which thus limits the number of undetectable particles. The percentage capture was calculated through linear interpolation, using pure PBS droplets (0% loading) and droplets containing particles before extraction (100% loading) as bottom and top reference values. As the particle distribution apparently varied markedly from one droplet to another, the capture percentage was averaged for 15 droplets for each velocity condition, and the standard deviation was determined using propagation of error formulas (Figure S4, Supporting Information). Droplet velocities were measured on videos with a constant frame rate of 50 fps using another custom MATLAB program that detects the centers of the droplets and calculates their coordinates in each frame. The velocities were then extracted, averaged over at least 10 droplets, and the standard deviations over these droplets were computed.

Co-Encapsulation of Single-Cells and Magnetic Particles: Dynabeads MyOne Streptavidin C1 (Invitrogen) were conjugated with oligo-dT30VN primers, as described previously,[38] and resuspended in 1.5× lysis/binding buffer composed of Tris-HCl pH 7.5 (150 mM), NaCl (750 mM), EDTA (15 mM), Triton X-100 (0.075% *w/v*), BSA (0.75% *w/v*), and RiboLock RNase Inhibitor (3 U $µL^{-1}$, Thermo Scientific). MDA-MB-231 breast cancer cells were cultured following standard procedures, then resuspended in PBS with 15% *v/v* Optiprep at 850 cells $µL^{-1}$. The bead and cell solutions were co-emulsified using the flow-focusing microfluidic device into ≈500 pL droplets, of which around 10% contained a cell. A bead/cell solution flow rate ratio of 2:1 and throughput of 350 Hz were maintained throughout droplet generation. Droplets were stored in home-made reservoirs on ice until reinjection.

On-Chip mRNA Purification and (RT)-qPCR Quantification: The droplets containing oligo-dT beads and the sample were reinjected in the magnetic microtweezer chip at a flow rate of 40 µL h^{-1}, yielding a throughput of 20 droplets passing through the tweezers per second. After separation of the magnetic particles by the tweezers, the droplets were passed through an intermediary reservoir equipped with a magnet to trap the clusters of magnetic particles. The emulsions were collected and broken using a 20% *v/v* solution of 1H,1H,2H,2H-perfluoro-1-octanol (Apollo Scientific) in Novec-7500 (3 M), and the quantities of gDNA/mRNA were assessed using (RT)-qPCR. The detailed PCR protocol, primer sequences, C_t values, and calibration curves are provided in Equation (SB.2) (Supporting Information).

Supporting Information

Supporting Information is available from the Wiley Online Library or from the author.

Acknowledgements

The authors acknowledge all members of the IPGG technological platform for their help with microfabrication, especially Olivier Lesage

for his support in photolithography and sputtering and Bertrand Cinquin for EDX spectrometry. They also thank Koceila Aizel for support with electroplating, and Fanny Tabarin and Aude Battistella for training them on cell and molecular biology (Institut Curie, UMR168), David Hrabovsky (MPBT platform, Sorbonne University) for magnetometry measurements, and Olivier Lefebvre (C2N, Univ. Paris-Saclay) for helpful advice on electroplating. This work was supported by the Institut Pierre-Gilles de Gennes (équipement d'excellence and LABEX, "Investissement d'avenir," program ANR-10-EQPX-34).

Conflict of Interest

The authors declare no conflict of interest.

Data Availability Statement

The data that support the findings of this study are available from the corresponding author upon reasonable request.

Keywords

droplet microfluidics, magnetic particles, single-cell analysis

Received: May 6, 2022
Revised: July 8, 2022
Published online:

[1] E. Shapiro, T. Biezuner, S. Linnarsson, *Nat. Rev. Genet.* **2013**, *14*, 618.
[2] K. Matuła, F. Rivello, W. T. S. Huck, *Adv. Biosyst.* **2020**, *4*, 1900188.
[3] A. M. Klein, L. Mazutis, I. Akartuna, N. Tallapragada, A. Veres, V. Li, L. Peshkin, D. A. Weitz, M. W. Kirschner, *Cell* **2015**, *161*, 1187.
[4] E. Z. Macosko, A. Basu, R. Satija, J. Nemesh, K. Shekhar, M. Goldman, I. Tirosh, A. R. Bialas, N. Kamitaki, E. M. Martersteck, J. J. Trombetta, D. A. Weitz, J. R. Sanes, A. K. Shalek, A. Regev, S. A. McCarroll, *Cell* **2015**, *161*, 1202.
[5] C. Zhu, S. Preissl, B. Ren, *Nat. Methods* **2020**, *17*, 11.
[6] P. Shahi, S. C. Kim, J. R. Haliburton, Z. J. Gartner, A. R. Abate, *Sci. Rep.* **2017**, *7*, 44447.
[7] V. M. Peterson, K. X. Zhang, N. Kumar, J. Wong, L. Li, D. C. Wilson, R. Moore, T. K. Mcclanahan, S. Sadekova, J. A. Klappenbach, *Nat. Biotechnol.* **2017**, *35*, 936.
[8] M. Stoeckius, C. Hafemeister, W. Stephenson, B. Houck-Loomis, P. K. Chattopadhyay, H. Swerdlow, R. Satija, P. Smibert, *Nat. Methods* **2017**, *14*, 865.
[9] S. Chen, B. B. Lake, K. Zhang, *Nat. Biotechnol.* **2019**, *37*, 1452.
[10] I. C. Macaulay, W. Haerty, P. Kumar, Y. I. Li, T. X. Hu, M. J. Teng, M. Goolam, N. Saurat, P. Coupland, L. M. Shirley, M. Smith, N. Van Der Aa, R. Banerjee, P. D. Ellis, M. A. Quail, H. P. Swerdlow, M. Zernicka-Goetz, F. J. Livesey, C. P. Ponting, T. Voet, *Nat. Methods* **2015**, *12*, 519.
[11] Y. Hu, K. Huang, Q. An, G. Du, G. Hu, J. Xue, X. Zhu, C. Y. Wang, Z. Xue, G. Fan, *Genome Biol.* **2016**, *17*, 88.
[12] M. Serra, D. Ferraro, I. Pereiro, J.-L. Viovy, S. Descroix, *Lab Chip* **2017**, *17*, 3979.
[13] E. Brouzes, T. Kruse, R. Kimmerling, H. H. Strey, *Lab Chip* **2015**, *15*, 908.
[14] R. Gao, Z. Cheng, A. J. Demello, J. Choo, *Lab Chip* **2016**, *16*, 1022.
[15] S. R. Doonan, R. C. Bailey, *Anal. Chem.* **2017**, *89*, 4091.
[16] Y. Fouillet, D. Jary, C. Chabrol, P. Claustre, C. Peponnet, *Microfluid. Nanofluid.* **2008**, *4*, 159.
[17] A. Rival, D. Jary, C. Delattre, Y. Fouillet, G. Castellan, A. Bellemin-Comte, X. Gidrol, *Lab Chip* **2014**, *14*, 3739.
[18] X. Shi, C. H. Chen, W. Gao, S. H. Chao, D. R. Meldrum, *Lab Chip* **2015**, *15*, 1059.
[19] A. Ali-Cherif, S. Begolo, S. Descroix, J.-L. Viovy, L. Malaquin, *Angew. Chem., Int. Ed.* **2012**, *51*, 10765.
[20] D. Ferraro, J. Champ, B. Teste, M. Serra, L. Malaquin, J.-L. Viovy, P. de Cremoux, S. Descroix, *Sci. Rep.* **2016**, *6*, 25540.
[21] M. Serra, T. D. Mai, A. L. Serra, M. C. Nguyen, A. Eisele, L. Perié, J. L. Viovy, D. Ferraro, S. Descroix, *Sens. Actuators, B* **2020**, *305*, 127346.
[22] M. Serra, E. Gontran, I. Hajji, L. Malaquin, J. Viovy, S. Descroix, D. Ferraro, *Adv. Mater. Technol.* **2020**, *5*, 1901088.
[23] J. Nguyen, D. V. Conca, J. Stein, L. Bovo, C. A. Howard, I. L. Garcia, *Proc. Natl. Acad. Sci. U. S. A.* **2019**, *116*, 2425.
[24] M. Glickman, P. Tseng, J. Harrison, T. Niblock, I. B. Goldberg, J. W. Judy, *J. Microelectromech. Syst.* **2011**, *20*, 842.
[25] P. Tseng, J. W. Judy, D. Di Carlo, *Nat. Methods* **2012**, *9*, 1113.
[26] J. Cottet, C. Vaillier, F. Buret, M. Frénéa-Robin, P. Renaud, *Biomicrofluidics* **2017**, *11*, 064111.
[27] N. Pamme, *Lab Chip* **2006**, *6*, 24.
[28] A. Van Reenen, A. M. De Jong, J. M. J. Den Toonder, M. W. J. Prins, *Lab Chip* **2014**, *14*, 1966.
[29] J. Faraudo, J. Camacho, *Colloid Polym. Sci.* **2010**, *288*, 207.
[30] B. Hallmark, N. J. Darton, D. Pearce, *Magnetic Nanopartics Biosensing Medicine*, Cambridge University Press, Cambridge, UK **2019**, pp. 151–171.
[31] J. Faraudo, J. S. Andreu, J. Camacho, *Soft Matter* **2013**, *9*, 6654.
[32] K. Yang, C. Lu, X. Zhao, R. Kawamura, *PLoS One* **2017**, *12*, e0188015.
[33] S. Torquato, T. M. Truskett, P. G. Debenedetti, *Phys. Rev. Lett.* **2000**, *84*, 2064.
[34] 10X Genomics website Q&A, *What fraction of mRNA transcripts are captured per cell?* **2022**.
[35] M. Glickman, T. Niblock, J. Harrison, I. B. Goldberg, P. Tseng, J. W. Judy, In *Solid State Sensors and Actuators Workshop*, Hilton Head Isl **2010**.
[36] C. Braïni, A. Mottolese, I. Ferrante, S. Monnier, C. Villard, *J. Vis. Exp.* **2018**, *2018*, e56923.
[37] O. J. Dressler, T. Yang, S. I. Chang, J. Choo, R. C. R. Wootton, A. J. Demello, *RSC Adv.* **2015**, *5*, 48399.
[38] I. C. Macaulay, M. J. Teng, W. Haerty, P. Kumar, C. P. Ponting, T. Voet, *Nat. Protoc.* **2016**, *11*, 2081.